JACS
JOURNAL OF THE AMERICAN CHEMICAL SOCIETY
Article
pubs.acs.org/JACS

Atomistic Mechanisms Underlying Selectivities in C_1 and C_2 Products from Electrochemical Reduction of CO on Cu(111)

Hai Xiao, Tao Cheng, and William A. Goddard, III*

Materials and Process Simulation Center (MSC) and Joint Center for Artificial Photosynthesis (JCAP), California Institute of Technology, Pasadena, California 91125, United States

Supporting Information

ABSTRACT: Practical environmental and energy applications of the electrochemical reduction of CO_2 to chemicals and fuels require far more efficient and selective electrocatalysts beyond the only working material Cu, but the wealth of experimental data on Cu can serve to validate any proposed mechanisms. To provide design guidelines, we use quantum mechanics to predict the detailed atomistic mechanisms responsible for C_1 and C_2 products on Cu. Thus, we report the pH dependent routes to the major products, methane and ethylene, and identify the key intermediates where branches to methanol, ketene, ethanol, acetylene, and ethane are kinetically blocked. We discovered that surface water on Cu plays a key role in the selectivity for hydrocarbon products over the oxygen-containing alcohol products by serving as a strong proton donor for electrochemical dehydration reductions. We suggest new experiments to validate our predicted mechanisms.

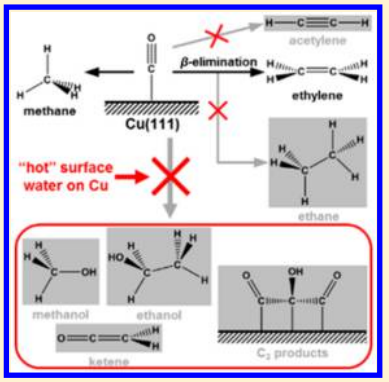

INTRODUCTION

Electrochemical reduction of CO_2 (CO_2RR) to chemicals and fuels provides both a promising industrial-scale means to reduce the carbon footprint under mild conditions and a candidate for energy storage of electrical power from intermittent renewable sources into stable chemical forms.[1] The only known electrode material that produces significant amounts of valuable products (primarily methane and ethylene, with minor alcohol products)[2−7] is copper, which suffers from high overpotentials and a lack of selectivity, precluding practical applications. In order to provide the basis for developing more efficient and selective electrocatalysts, we report here the complete mechanistic understanding of the pH dependent processes on Cu based on grand canonical quantum mechanics (GC-QM) including solvation.

In the course of CO_2RR on Cu, CO is produced with the lowest overpotential and the electrochemical reduction of CO (CORR) on Cu delivers the same product spectrum as that of CO_2.[8,9] Thus, CORR determines the overpotentials and selectivities for additionally reduced products from CO_2RR, so we focus here on CORR. Cu(111) serves as a model electrocatalyst that delivers the essential chemistry of CORR,[10] and it has been confirmed to be stable under electrochemical working conditions,[11] so we focus here on CORR on Cu(111).

Several computational investigations with density functional theory (DFT) methods have proposed mechanisms for CORR on Cu surfaces.[12−19] However, early studies ignored reaction barriers and made only very approximate corrections for the effect of solvation.

In 2013, Nie et al.[14,15] reported the first study that includes transition states (TS) for CORR on Cu(111) but with a very limited description of solvation. They concluded that COH_{ad} is the kinetically dominant key intermediate, leading to CH_x (x = 0−4) species sequentially, and proposed that C_2H_4 formation occurs from the $CH_{2,ad}$ step, which is contradicted by the experimental conclusion that pathways to CH_4 and C_2H_4 branch at an early stage of CORR.[20,21] Indeed, in 2015, Montoya et al.[16] predicted the barriers of CO dimerization on Cu(111) and (100) to be sufficiently low that C−C coupling should take place at the very beginning of CORR. This study used an oversimplified charged water layer to mimic the electrochemical environment for highly negative applied potentials.

However, all previous calculations were compromised by oversimplified treatments of solvation and the assumption that the number of electrons (N_e) remains constant along each elementary step, whereas the electrochemical half-cells are open systems operating at applied constant electrochemical potentials (μ_e). Such calculations with constant N_e admit large variations in μ_e,[14] which introduces significant deviations through the $\mu_e N_e$ contribution to free energies. Such inconsistency precludes quantitative predictions.

We recently reported the first quantum mechanics (QM) study with explicitly constant μ_e for CORR[18] which has now been validated by Goodpaster et al.[19] Our GC-QM calculations were realized within the framework of joint DFT (JDFT),[22] that introduces solvation effects using the CANDLE implicit model[23] and retains a fixed external potential by variationally optimizing N_e along the reaction path (the resulting net charge is handled by ionic screening).[24] These GC-QM studies allowed us to predict the initial steps for pH dependent mechanisms underlying the competition between C_1 and C_2 pathways on Cu(111). We

Received: July 2, 2016
Published: December 7, 2016

DOI: 10.1021/jacs.6b06846
J. Am. Chem. Soc. 2017, 139, 130−136

found that the C_1 pathway dominates kinetically through COH_{ad} formation at low pH, whereas the C_2 pathway opens up by direct CO_{ad} dimerization at high pH, while at neutral pH we find a novel CO−COH coupling that shares the common intermediate COH_{ad} with the C_1 pathway.[18] On the basis of the GC-QM, we predicted the onset potentials (U) for C_1 and C_2 products, in excellent agreement with experiment (within 0.06 V) for pH 1, 7, and 12.[18,25,26] We should note that possible complications in real experiments might compromise the comparison, including the difference between local and bulk pH and imperfections present in the electrode surface. Nevertheless, these recent studies[18,19] examined only the first few steps of CORR, providing overpotentials and selectivity for single-carbon vs multicarbon products. A complete picture of the final product spectrum, particularly the selectivity for hydrocarbon vs alcohol products, has not previously been established.

Here we use these GC-QM methods to determine the complete C_1 and C_2 pathways for CORR on Cu(111). A very important element of our new mechanisms is the **critical role of surface bound H_2O in electrochemical dehydration reduction**. Starting from our previous work establishing that C_1 pathways up to $CHOH_{ad}$ are enabled for pH $\leq$ 7 while C_2 pathways up to $COCOH_{ad}$ are accessible for pH $\geq$ 7,[18] we now investigate the constant μ_e free energy barriers for all possible competing pathways to provide the roadmap of pH dependent routes to the major products and to identify the key intermediates at which branches to other products are blocked. Then, we use our new mechanism to suggest experiments using probe molecules to experimentally validate details of our mechanisms. A critical point here is our discovery that **surface water on Cu provides the key to selectivity of hydrocarbon vs alcohol products**. The Supporting Information provides reaction barriers and energies for all competing pathways studied, of which only the dominant ones are discussed here.

COMPUTATIONAL DETAILS

The calculations were first performed with the VASP package,[27−29] using the PBE flavor[30] of DFT and the projector augmented wave (PAW) method[31] to account for core−valence interactions. The kinetic energy cutoff for plane wave expansions was set to 400 eV, and reciprocal space was sampled by the Γ-centered Monkhorst−Pack scheme with a grid of 3 × 3 × 1. The Cu(111) surface slabs were constructed with three layers (bottom layer fixed) using the PBE-optimized lattice parameter of 3.635 Å, with vacuum layers of at least 15 Å, and the slab sizes are 4 × 4, 4 × 5, or 5 × 5, depending on the adsorbates for low coverage limit. Please refer to the Appendix of the Supporting Information for coordinates of all structures studied.

The convergence criteria are 1×10^{-5} and 1×10^{-7} eV energy differences for solving for the electronic wave function for local minima (initial states (IS) and final states (FS)) and TS, respectively. The Methfessel−Paxton smearing of second order with a width of 0.1 eV was applied. All IS, TS, and FS geometries (atomic coordinates) are converged to within 3×10^{-2} eV/Å for maximal components of forces. The TS search was conducted by using the climbing image nudged elastic band (CI-NEB) method[32] to generate initial guess geometries, followed by the dimer method[33] to converge to the saddle points.

Zero-point energies (ZPE) and enthalpy and entropy contributions to free energies at room temperature (298.15 K) were calculated from vibrational modes of surface species, which were computed with density functional perturbation theory (DFPT). Note that very low frequency modes were obtained in some cases, because the explicit water molecules are not properly constrained by the hydrogen bonding network present in water bulk. Such low frequency modes can cause unphysically large entropy contributions, so they were reset to a threshold value of 60 cm^{-1}, corresponding to the acoustic translational mode of the six-member rings in water bulk.[34,35]

For steps where the surface H model was used to locate TSs, ISs were referenced back to with the $H^+(H_3O^+/H_2O) + e^-$ pair through free energy differences between the surface H and $H_2(g)$, based on the half-cell reactions,

$$H_3O^+ + e^- = {}^1/_2 H_2(g) + H_2O \times \mathrm{pH\ (eV)}, \quad \Delta G = 0.0592$$

$$H_2O + e^- = {}^1/_2 H_2(g) + OH^- \times \mathrm{pH\ (eV)}, \quad \Delta G = 0.0592$$

Thus, the pH effect is introduced into the free energy profiles with the reference. In addition to vibrational contributions, the translational and rotational contributions to the free energy of $H_2(g)$ were included, assuming the ideal gas model. For the models where H_3O^+ is explicitly present or H_2O acts as the proton source with releasing OH^- (see below), the pH enters the free energy profiles naturally as the reactant or product, similar to other work.[36]

The explicit constant electrochemical potential (μ_e) calculations with the implicit CANDLE solvation model[23] were performed upon all IS, TS, and FS geometries using JDFTx.[37] The GBRV[38] ultrasoft pseudopotentials (USPP) were used, with a plane wave cutoff of 544 eV (20 au). All other settings are similar to those in VASP calculations. The ionic screening of net charges resulting from the constant μ_e condition was achieved with cation (0.1 M K^+) and anion (0.1 M F^-) components in the fluid model[24] under the JDFT framework.[22] The algorithm employed by JDFTx variationally minimizes the grand free energy at fixed electron chemical potential with respect to Kohn−Sham orbitals,[39] fluid bound charge, and an auxiliary Hamiltonian for the occupations.[40] Previously, we have found that the relative free energies (barriers $\Delta G^{\ddagger}$ and reaction energies ΔG) are linearly dependent on the applied potential U for $|U| <$ ~2 V (vs standard hydrogen electrode (SHE)),[18] so the U-dependence of all $\Delta G^{\ddagger}$ and ΔG was calculated assuming a linear relationship between U = 0.0 and −1.2 V. Note that here all U's are referenced to SHE.

The minimal onset potentials U_{min} were then determined by solving the equation $e|U_{min}| = \max(\Delta G^{\ddagger}, \Delta G)$,[18] which assumes that the energy of eU brought by the incoming electron is fully utilized to overcome the highest point on the free energy surface and thus drive the reaction. The comparison between $\Delta G^{\ddagger}$ and ΔG is necessary because, for some ranges of U, the TS can be lower in energy than the final state, making the step a simple uphill process.

RESULTS AND DISCUSSION

In examining each electrochemical reduction step, we assume that the proton source (H_3O^+ or H_2O) and electron source are refilled in advance, in the form of surface H that is taken as the starting point to locate the TS. $\Delta G^{\ddagger}$ and ΔG are later corrected by referencing back to the $H^+(H_3O^+/H_2O) + e^-$ pair through H_2. This surface H model is reasonable for finding the lowest energy barrier pathway, particularly for hydrogenation of C atoms

DOI: 10.1021/jacs.6b06846
J. Am. Chem. Soc. 2017, 139, 130−136

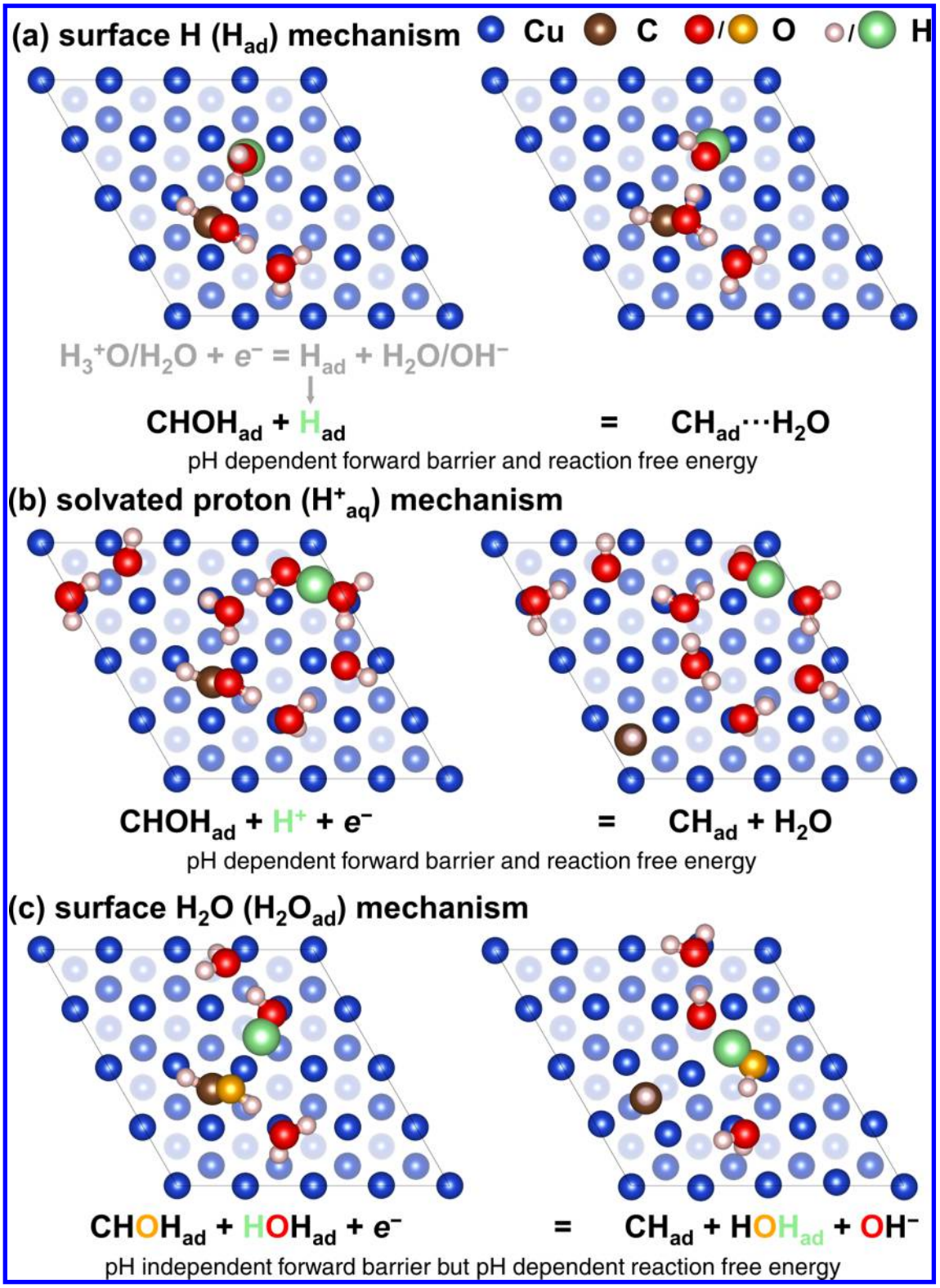

Figure 1. Three mechanisms for electrochemical dehydration reduction illustrated with the $CHOH_{ad}$ case: (a) surface H (H_{ad}), (b) solvated proton (H^+_{aq}), and (c) surface H_2O (H_2O_{ad}). In each case, the H initiating the reaction is shown in light green. Note that in part b the final position of CH_{ad} has moved substantially from the initial position of $CHOH_{ad}$. This is where CH_{ad} ends up in our minimization procedure. We assume that it is due to the repulsion between CH_{ad} and the lone pair on H_2O being formed.

(which are partially positive charged, and thus prefer the surface H which acquires a partially negative charge from the metal).

Our studies using QM based molecular dynamics (QMD) including five layers of explicit solvent and a proton[17] showed that, at low pH, the dehydration step through hydrogenation of the hydroxyl group of the $CHOH_{ad}$ intermediate favors direct protonation mediated by aqueous water, instead of the surface H. There we speculated that, at neutral and high pH, "hot" surface

DOI: 10.1021/jacs.6b06846
J. Am. Chem. Soc. 2017, 139, 130−136

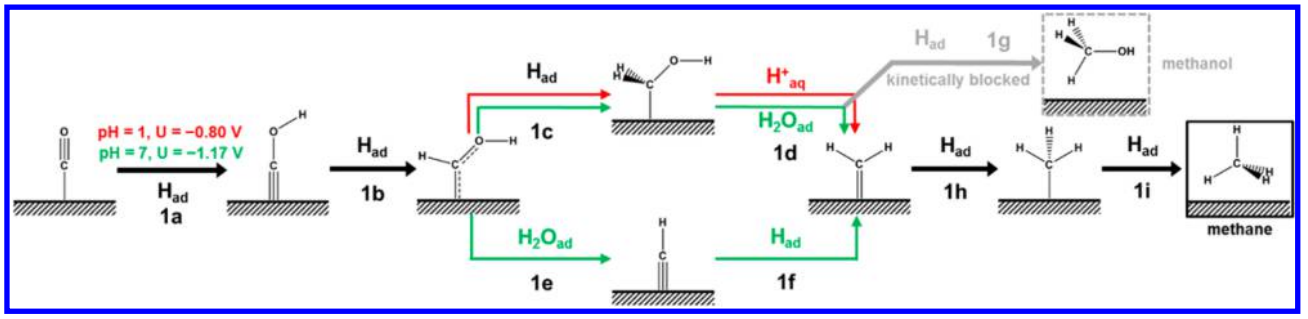

Figure 2. Predicted complete pH dependent pathways for C_1 products.

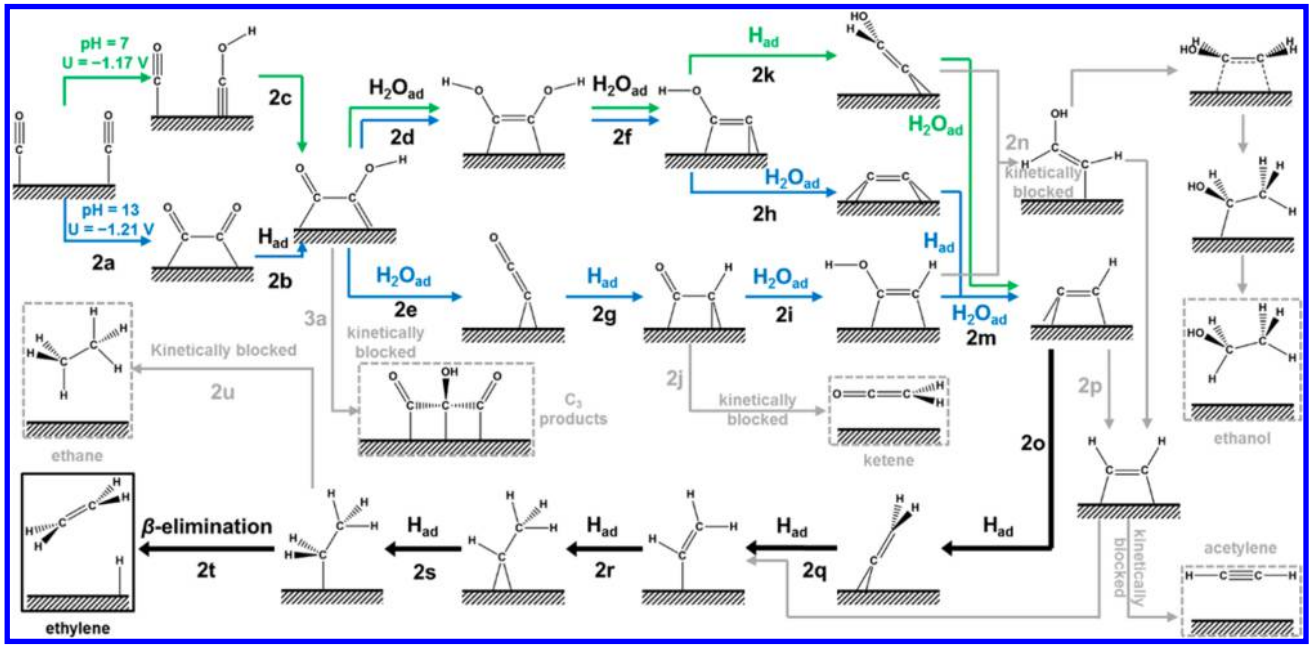

Figure 3. Predicted complete pH dependent pathways for C_2 products.

H_2O plays the essential role as the direct proton source, because the negatively charged O atom in the hydroxyl group is attractive to the positively charged proton in either H_3O^+ or "hot" surface H_2O.

Herein we use GC-QM to examine the following:

(a) The standard surface H (H_{ad}) Langmuir–Hinshelwood (LH) mechanism illustrated in Figure 1a, in which H_{ad} activates an on-top aqueous water to provide the proton to the hydroxyl group.

(b) The solvated proton (H^+_{aq}) Eley–Rideal (ER) mechanism illustrated in Figure 1b, where the excess proton in solution arrives at the hydroxyl group via a Grotthuss mechanism, as observed in our previous QMD calculations on Cu(100).[17]

(c) A new surface H_2O (H_2O_{ad}) LH mechanism not previously considered. This "hot H_2O" mechanism is illustrated in Figure 1c, where H_2O_{ad} donates a proton directly to the hydroxyl group (or in some cases mediated by an aqueous water via a Grotthuss mechanism), leaving behind OH bonded to the metal. The reason that it is favorable for a H_2O_{ad} to donate a proton is that the final OH_{ad} is bound by 2.3 eV to the Cu surface, whereas H_2O_{ad} is bound by less than 0.1 eV. Under constant μ_e calculations with JDFT, the product OH_{ad} turns into OH^-.

Figure 1 illustrates these three mechanisms for the $CHOH_{ad}$ dehydration step. A notable characteristic of these mechanisms is the pH dependence:

(a) For the H_{ad} mechanism, the formation of the H_{ad} next to the reactant involves implicitly either H_3O^+ or OH^-, so both $\Delta G^{\ddagger}$ and ΔG are pH dependent.

(b) The same applies to the H^+_{aq} mechanism, since the proton enters directly the reactant side.

(c) However, for our new H_2O_{ad} mechanism, $\boldsymbol{\Delta G^{\neq}}$ **is generally pH independent**, while the OH^- present at the product side makes ΔG pH dependent. This makes the H_2O_{ad} mechanism advantageous for kinetics at higher pH.

At pH 1 and 7 (Figure 2), we showed previously that the first step (1a) is hydrogenation of CO_{ad} by H_{ad} to form COH_{ad} with a predicted rate limiting $U = -0.80$ and -1.17 V (vs $U_{exp} = -0.76$ and -1.21 V), respectively, and the next step (1b) is the formation of $CHOH_{ad}$ by the H_{ad} mechanism.[18]

At pH 1, the hydrogenation of $CHOH_{ad}$ to CH_2OH_{ad} (1c) follows dominantly, while the dehydration of $CHOH_{ad}$ driven by the H^+_{aq} mechanism (see Table S1 in the Supporting Information) is kinetically blocked, with a barrier higher by 0.16 eV (rate lower by a factor of 500). This is due to the conjugation of the C–O and C–Cu bonds in $CHOH_{ad}$, making the C–O bond relatively strong (1.37 Å).

DOI: 10.1021/jacs.6b06846
J. Am. Chem. Soc. 2017, 139, 130–136

At pH 7, the hydrogenation step (1c) remains kinetically accessible, but the dehydration path (1e) to CH_{ad} by the H_2O_{ad} mechanism forks to a competing branch, with a barrier slightly lower by 0.03 eV.

For CH_2OH_{ad}, the C−O bond (1.45 Å) is weaker (a normal C−O single bond), and the subsequent dehydration to $CH_{2,ad}$ (1d) by either the H^+_{aq} mechanism at pH 1 or the H_2O_{ad} mechanism at pH 7 kinetically dominates over further hydrogenation toward methanol production, with barriers lower by 0.05 and 0.29 eV, respectively (rates down by factors of 7 and 80 000). The resulting $CH_{2,ad}$ proceeds to the final methane product using H_{ad} for both pHs. Hence, at pH 1 and 7, CH_2OH_{ad} is the key intermediate that decides the selectivity of CORR on Cu(111) for methane over methanol, and the *"hot" surface water plays the critical role in the dehydration step at neutral pH*, the most common scenario.

At pH 13 (Figure 3), we showed previously that the first step (2a) is dimerization of CO_{ad} to form $OC{-}CO_{ad}$ with a predicted rate limiting $U = -1.21$ V (vs $U_{exp} = -1.26$ V), followed by the hydrogenation (2b) with H_{ad} to form $OC{-}COH_{ad}$.[18] We show here that the next step has two competing branches with comparable kinetics: formation of $HOC{=}COH_{ad}$ (2d) by acquiring a proton from a "hot" surface H_2O with a pH independent $\Delta G^{\ddagger}$ of 0.01 eV but an uphill pH dependent ΔG of 0.83 eV and formation of $O{=}C{=}C_{ad}$ (2e) by the H_2O_{ad} mechanism with $\Delta G^{\ddagger}$ of 0.83 eV. Thus, the "hot" surface water plays an essential role in both the dehydration and the protonation of the C═O group. Here the coupling to a third CO_{ad} (3a) to initiate C_3 products with a $\Delta G^{\ddagger}$ of 1.00 eV is blocked kinetically by both branches.

Following formation of $HOC{=}COH_{ad}$, the next step (2f) is dehydration to $HOC{=}C_{ad}$ via the H_2O_{ad} mechanism with $\Delta G^{\ddagger}$ = 0.99 eV (pH independent). This mutes the hydrogenation to the $HO(CH){-}COH_{ad}$ channel (not shown) which has a pH dependent $\Delta G^{\ddagger}$ = 1.62 eV. Then, $HOC{=}C_{ad}$ undergoes dehydration (2h) to a surface dicarbide state ($C{=}C_{ad}$) with $\Delta G^{\ddagger}$ = 1.10 eV, instead of hydrogenation (2k) to $HO(CH){=}C_{ad}$ ($\Delta G^{\ddagger}$ = 1.43 eV due to the pH increase). Then, $C{=}C_{ad}$ is further hydrogenated (2m) by H_{ad} to form $C{=}CH_{ad}$.

The formation of $O{=}C{=}C_{ad}$ via H_2O_{ad} (2e) then proceeds to $OC{-}CH_{ad}$ via H_{ad} (2g), followed by protonation of the C═O group by H_2O_{ad} (2i) to form $HOC{=}CH_{ad}$, with an uphill ΔG = 0.86 eV. The production of ketene (2j) is kinetically forbidden with $\Delta G^{\ddagger}$ = 1.47 eV. Dehydration of $HOC{=}CH_{ad}$ with H_2O_{ad} (2m) forms CCH_{ad} (2m) with $\Delta G^{\ddagger}$ = 1.16 eV. This constitutes convergence with the 2d-2f-2h-2m pathways. Further hydrogenation (2n) to form $HO(CH){=}CH_{ad}$ which would lead to ethanol production has $\Delta G^{\ddagger}$ = 1.46 eV, making it kinetically forbidden. Thus, "hot" surface water eliminates both ketene and ethanol products.

At pH 7, we showed previously that the C_2 pathways are accessed via a novel OC—COH coupling (2c) that shares the common intermediate COH_{ad} with the C_1 pathways.[18] We show here that the C_2 pathway leads to formation of $HOC{=}COH_{ad}$ via H_2O_{ad} (2d) just as for pH 13 but with a lower uphill pH dependent ΔG of 0.47 eV, which then blocks kinetically the branch to $O{=}C{=}C_{ad}$ formation (2e). Just as for pH 13, the C_2 pathway is followed by production of $HOC{=}C_{ad}$ via H_2O_{ad} (2f). The next step at pH 7 is hydrogenation with H_{ad} (2k) to form $HO(CH){=}C_{ad}$ with $\Delta G^{\ddagger}$ = 1.08 eV, instead of the dehydration by H_2O_{ad} (2h) to form $C{=}C_{ad}$ that occurs at pH 13. Next, H_2O_{ad} drives further dehydration (2m) of $HO(CH){=}C_{ad}$ to $C{=}CH_{ad}$ ($\Delta G^{\ddagger}$ = 0.86 eV). This kinetically blocks the hydrogenation pathway (2n) to $HO(CH){=}CH_{ad}$ ($\Delta G^{\ddagger}$ = 1.13 eV) that would produce ethanol. Thus, at neutral pH, the "hot" surface water plays the key role in ruling out both C_3 and ethanol products. This provides a hint that, to promote alcohol production, we should destabilize the H_2O_{ad} pathways.

Following $HC{=}C_{ad}$, further electrochemical reduction kinetically favors formation of $H_2C{=}C_{ad}$ via H_{ad} (2o) with $\Delta G^{\ddagger}$ lower by 0.20 eV than for formation of $HC{=}CH_{ad}$. Even if $HC{=}CH_{ad}$ were formed, the nonelectrochemical desorption of acetylene has ΔG = 1.0 eV, making it slow, and $HC{=}CH_{ad}$ favors the electrochemical hydrogenation to form $H_2C{=}CH_{ad}$. Thus, we predict that acetylene is *not* formed under these conditions, which is consistent with experiment.[6] Sequential hydrogenation of $H_2C{=}C_{ad}$ with H_{ad} (2q-2r-2s) leads to $CH_3CH_{2,ad}$. Surprisingly, the last step is nonelectrochemical β-elimination (2t with $\Delta G^{\ddagger}$ = 0.59 eV) that delivers the final ethylene product, leading to very fast kinetics, with a turn over frequency (TOF) of 7×10^2 s^{-1}, based on the Eyring−Polanyi equation. No ethane should be produced, since further hydrogenation (2u) has a barrier of 0.88 eV at pH 7 and 1.23 eV at pH 13. In fact, ethane has been reported occasionally as a minor product from CORR on specifically designed nanostructured Cu electrodes.[41−43] This suggests that the morphology of the Cu surface might be tuned to suppress the fast β-elimination process to enable ethane production.

In our previous work,[18] we showed that our GC-QM methodology leads to onset potentials within 0.06 eV of experiment for pH 1, 7, and 12, validating the accuracy of the level of DFT theory, the CANDLE solvation model, and the GC-QM method. In order to provide additional experimental tests of our very detailed mechanisms for subsequent product formation during CORR on Cu(111), we propose here several specific probe molecules that could be introduced to access new pathways at each pH while avoiding the constraint in CORR whereby pH selects C_1 or C_2 pathways. Figure 4 shows three candidates:

(a) formaldehyde to probe the key intermediate CH_2OH_{ad} that selects methane production over methanol in C_1 pathways
(b) ketene to probe the predicted intermediate $HO(CH){=}CH_{2,ad}$ that leads exclusively to ethanol production once formed
(c) acetylene for verifying the predicted mechanisms for selectivity of C_2H_4 vs C_2H_6

With formaldehyde, we expect to form a surface methoxy intermediate CH_3O_{ad} by the H_{ad} mechanism, which leads to methanol production exclusively, as suggested previously.[14,15] In contrast, the target CH_2OH_{ad} pathways are not switched on until pH ≥ 10.1, due to the potential limiting step of dehydration to $CH_{2,ad}$, at which point the methane production has comparable kinetics (see Tables S1 and S3 in the Supporting Information). This might resolve an apparent contradiction in the experimental literature: Schouten et al. reported methanol as the only major product from electrochemical reduction of HCHO on Cu at pH 7 using a K_2HPO_4/KH_2PO_4 buffer,[20] but a more recent experiment reported both methane and alcohol as major products.[44] Here a main difference in the setup is the use of $KHCO_3$ solution, which gives a pH of 8.2 and does not form a buffer without input of CO_2. Thus, the electrochemical reduction of HCHO takes place at basic pH and even higher local pH due to consumption of protons. Therefore, our predicted mechanisms fit both experiments. Note also that our predicted U =

DOI: 10.1021/jacs.6b06846
J. Am. Chem. Soc. 2017, 139, 130−136

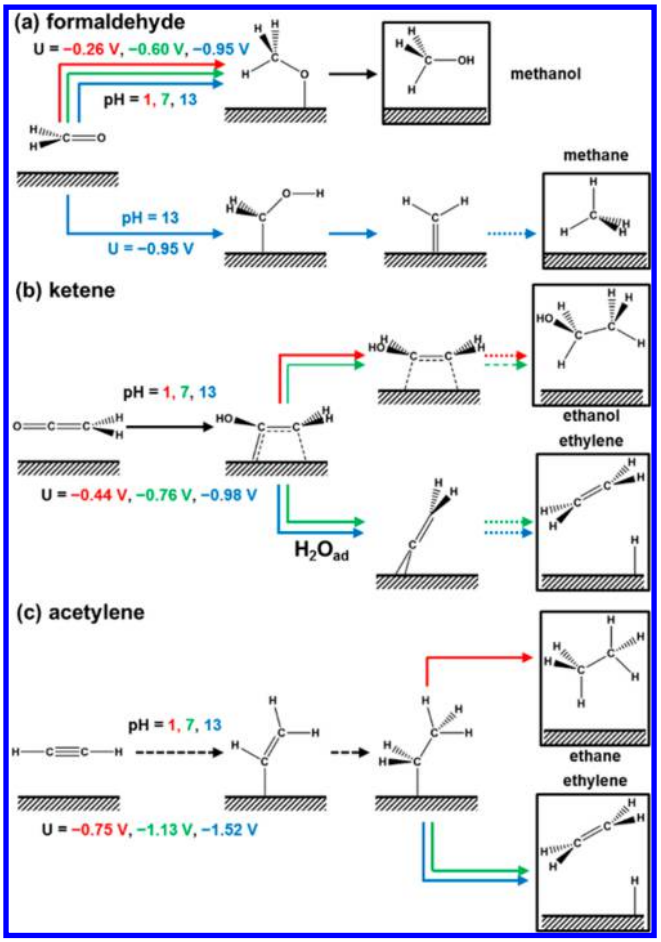

Figure 4. Proposed experimental validations of our proposed mechanisms by introducing probe molecules (a) formaldehyde, (b) keten, and (c) acetylene (with their predicted pH dependent product spectra). These studies would probe and validate (hopefully) our predicted CORR mechanisms. Note that the predicted onset potentials *U* are referenced to SHE.

−0.60 V for formation of methanol at pH 7 matches well the reported experimental value of −0.6 to −0.7 V.[20]

When ketene is fed at acidic pH, the pathways to target $HOCHCH_{2,ad}$ are kinetically favored, and thus, our prediction is that ethanol is the only final product. However, as pH increases to 7, a new pathway of dehydrating $HOCCH_{2,ad}$ to $H_2C{=}C_{ad}$ becomes slightly more favored kinetically, again through the H_2O_{ad} mechanism, and at basic pH, this route to ethylene production is totally dominant (see Table S3 in the Supporting Information). This demonstrates again that the "hot" surface water promotes hydrocarbon products over alcohol products.

Feeding acetylene produces no pH dependent branches, until it reaches our target intermediate $CH_2CH_{3,ad}$, at which we predict production ethane at acidic pH, with $\Delta G^{\ddagger} = 0.52$ eV for the final hydrogenation step, which is slightly lower than the $\Delta G^{\ddagger} = 0.57$ eV for the β-elimination process. At neutral and basic pH, the final hydrogenation to ethane is kinetically blocked, just as in CORR. Experimental confirmation would validate our prediction that the absence of ethane in the product spectrum is due to the combination of the fast β-elimination to form ethylene and the constraint in CORR that C_2 pathways are only enabled at neutral and basic pH.

SUMMARY

Summarizing, we present a complete roadmap to the mechanisms for CORR on Cu(111) that we expect to be valuable for developing new selective catalysts. Using the GC-QM for computational electrochemistry, we predict the full mechanistic description of C_1 and C_2 pathways in CORR on Cu(111) that explains the selectivity of methane vs methanol and the selectivity of ethylene vs ketene, ethanol, acetylene, and ethane. In addition, we propose new experiments to provide direct experimental tests of our detailed mechanisms. The introduction of probe molecules can insert into the mechanisms at specific spots to modify product distributions. This will allow detailed experimental checks on key intermediates in our predicted mechanisms.

An important discovery here is the critical role of surface H_2O on Cu in promoting dehydration and thus controlling the selectivity for hydrocarbon products, over oxygen-containing alcohol products. We expect this concept to provide an important principle in designing a new electrocatalyst to promote selectivity for liquid fuel oxygenates by modifying the "hotness" of surface water (for example, nanoscale sculpting of the surface).

ASSOCIATED CONTENT

Supporting Information

The Supporting Information is available free of charge on the ACS Publications website at DOI: 10.1021/jacs.6b06846.

Reaction barriers and energies for all pathways considered and coordinates for all structures studied (PDF)

AUTHOR INFORMATION

Corresponding Author

*wag@wag.caltech.edu

ORCID

Hai Xiao: 0000-0001-9399-1584

Tao Cheng: 0000-0003-4830-177X

William A. Goddard III: 0000-0003-0097-5716

Notes

The authors declare no competing financial interest.

ACKNOWLEDGMENTS

This work was supported by the Joint Center for Artificial Photosynthesis, a DOE Energy Innovation Hub, supported through the Office of Science of the U.S. Department of Energy under Award No. DE-SC0004993. We are grateful to Dr. Ravishankar Sundararaman, Dr. Robert J. Nielsen, and Prof. Manuel P. Soriaga for helpful discussions. The calculations were carried out on the Zwicky (Caltech) computing resource.

REFERENCES

(1) Zhu, D. D.; Liu, J. L.; Qiao, S. Z. *Adv. Mater.* **2016**, *28*, 3423.
(2) Hori, Y.; Kikuchi, K.; Suzuki, S. *Chem. Lett.* **1985**, *14*, 1695.
(3) Hori, Y.; Wakebe, H.; Tsukamoto, T.; Koga, O. *Electrochim. Acta* **1994**, *39*, 1833.
(4) Hori, Y. In *Modern Aspects of Electrochemistry*; Vayenas, C., White, R., Gamboa-Aldeco, M., Eds.; Springer: New York, 2008; Vol. *42*, p 89.
(5) Gattrell, M.; Gupta, N.; Co, A. *J. Electroanal. Chem.* **2006**, *594*, 1.
(6) Kuhl, K. P.; Cave, E. R.; Abram, D. N.; Jaramillo, T. F. *Energy Environ. Sci.* **2012**, *5*, 7050.
(7) Kuhl, K. P.; Hatsukade, T.; Cave, E. R.; Abram, D. N.; Kibsgaard, J.; Jaramillo, T. F. *J. Am. Chem. Soc.* **2014**, *136*, 14107.

DOI: 10.1021/jacs.6b06846
J. Am. Chem. Soc. 2017, 139, 130−136

(8) Hori, Y.; Murata, A.; Takahashi, R.; Suzuki, S. *J. Am. Chem. Soc.* **1987**, *109*, 5022.
(9) Hori, Y.; Takahashi, R.; Yoshinami, Y.; Murata, A. *J. Phys. Chem. B* **1997**, *101*, 7075.
(10) Hori, Y.; Takahashi, I.; Koga, O.; Hoshi, N. *J. Mol. Catal. A: Chem.* **2003**, *199*, 39.
(11) Kim, Y.-G.; Javier, A.; Baricuatro, J. H.; Torelli, D.; Cummins, K. D.; Tsang, C. F.; Hemminger, J. C.; Soriaga, M. P. *J. Electroanal. Chem.* **2016**, *780*, 290.
(12) Peterson, A. A.; Abild-Pedersen, F.; Studt, F.; Rossmeisl, J.; Norskov, J. K. *Energy Environ. Sci.* **2010**, *3*, 1311.
(13) Calle-Vallejo, F.; Koper, M. T. M. *Angew. Chem., Int. Ed.* **2013**, *52*, 7282.
(14) Nie, X.; Esopi, M. R.; Janik, M. J.; Asthagiri, A. *Angew. Chem., Int. Ed.* **2013**, *52*, 2459.
(15) Nie, X.; Luo, W.; Janik, M. J.; Asthagiri, A. *J. Catal.* **2014**, *312*, 108.
(16) Montoya, J. H.; Shi, C.; Chan, K.; Nørskov, J. K. *J. Phys. Chem. Lett.* **2015**, *6*, 2032.
(17) Cheng, T.; Xiao, H.; Goddard, W. A. *J. Phys. Chem. Lett.* **2015**, *6*, 4767.
(18) Xiao, H.; Cheng, T.; Goddard, W. A.; Sundararaman, R. *J. Am. Chem. Soc.* **2016**, *138*, 483.
(19) Goodpaster, J. D.; Bell, A. T.; Head-Gordon, M. *J. Phys. Chem. Lett.* **2016**, *7*, 1471.
(20) Schouten, K. J. P.; Kwon, Y.; van der Ham, C. J. M.; Qin, Z.; Koper, M. T. M. *Chem. Sci.* **2011**, *2*, 1902.
(21) Roberts, F. S.; Kuhl, K. P.; Nilsson, A. *Angew. Chem., Int. Ed.* **2015**, *54*, 5179.
(22) Petrosyan, S. A.; Rigos, A. A.; Arias, T. A. *J. Phys. Chem. B* **2005**, *109*, 15436.
(23) Sundararaman, R.; Goddard, W. A. *J. Chem. Phys.* **2015**, *142*, 064107.
(24) Letchworth-Weaver, K.; Arias, T. A. *Phys. Rev. B: Condens. Matter Mater. Phys.* **2012**, *86*, 075140.
(25) Schouten, K. J. P.; Qin, Z.; Gallent, E. P.; Koper, M. T. M. *J. Am. Chem. Soc.* **2012**, *134*, 9864.
(26) Schouten, K. J. P.; Pérez Gallent, E.; Koper, M. T. M. *J. Electroanal. Chem.* **2014**, *716*, 53.
(27) Kresse, G.; Hafner, J. *Phys. Rev. B: Condens. Matter Mater. Phys.* **1993**, *47*, 558.
(28) Kresse, G.; Furthmuller, J. *Comput. Mater. Sci.* **1996**, *6*, 15.
(29) Kresse, G.; Furthmuller, J. *Phys. Rev. B: Condens. Matter Mater. Phys.* **1996**, *54*, 11169.
(30) Perdew, J. P.; Burke, K.; Ernzerhof, M. *Phys. Rev. Lett.* **1996**, *77*, 3865.
(31) Kresse, G.; Joubert, D. *Phys. Rev. B: Condens. Matter Mater. Phys.* **1999**, *59*, 1758.
(32) Henkelman, G.; Uberuaga, B. P.; Jónsson, H. *J. Chem. Phys.* **2000**, *113*, 9901.
(33) Henkelman, G.; Jónsson, H. *J. Chem. Phys.* **1999**, *111*, 7010.
(34) Bertie, J. E.; Whalley, E. *J. Chem. Phys.* **1967**, *46*, 1271.
(35) Liu, H.; Wang, Y.; Bowman, J. M. *J. Phys. Chem. B* **2013**, *117*, 10046.
(36) Zhao, M.; Anderson, A. B. *Electrochem. Commun.* **2016**, *69*, 64.
(37) Sundararaman, R.; Gunceler, D.; Letchworth-Weaver, K.; Schwarz, K. A.; Arias, T. A. *JDFTx*, 2012, available from http://jdftx.sourceforge.net.
(38) Garrity, K. F.; Bennett, J. W.; Rabe, K. M.; Vanderbilt, D. *Comput. Mater. Sci.* **2014**, *81*, 446.
(39) Arias, T. A.; Payne, M. C.; Joannopoulos, J. D. *Phys. Rev. Lett.* **1992**, *69*, 1077.
(40) Freysoldt, C.; Boeck, S.; Neugebauer, J. *Phys. Rev. B: Condens. Matter Mater. Phys.* **2009**, *79*, 241103.
(41) Li, C. W.; Kanan, M. W. *J. Am. Chem. Soc.* **2012**, *134*, 7231.
(42) Ma, M.; Djanashvili, K.; Smith, W. A. *Angew. Chem., Int. Ed.* **2016**, *55*, 6680.
(43) Dutta, A.; Rahaman, M.; Luedi, N. C.; Mohos, M.; Broekmann, P. *ACS Catal.* **2016**, *6*, 3804.
(44) Javier, A.; Chmielowiec, B.; Sanabria-Chinchilla, J.; Kim, Y.-G.; Baricuatro, J. H.; Soriaga, M. P. *Electrocatalysis* **2015**, *6*, 127.

DOI: 10.1021/jacs.6b06846
J. Am. Chem. Soc. 2017, 139, 130−136